Dynamics of Inelastic Scattering of OH Radicals from Reactive and Inert Liquid Surfaces

ARTICLE *in* THE JOURNAL OF PHYSICAL CHEMISTRY C · JULY 2008

Impact Factor: 4.77 · DOI: 10.1021/jp8024683

4 AUTHORS:

Paul A.J. Bagot
University of Oxford
42 PUBLICATIONS **561** CITATIONS
SEE PROFILE

Carla Kidd
University of Leeds
12 PUBLICATIONS **186** CITATIONS
SEE PROFILE

Matthew L Costen
Heriot-Watt University
60 PUBLICATIONS **1,009** CITATIONS
SEE PROFILE

Kenneth G Mckendrick
Heriot-Watt University
91 PUBLICATIONS **1,468** CITATIONS
SEE PROFILE

Dynamics of Inelastic Scattering of OH Radicals from Reactive and Inert Liquid Surfaces

Paul A. J. Bagot, Carla Waring, Matthew L. Costen, and Kenneth G. McKendrick*

School of Engineering and Physical Sciences, Heriot-Watt University, Edinburgh, EH14 4AS, United Kingdom

Received: March 20, 2008; Revised Manuscript Received: April 30, 2008

The inelastic scattering of gas-phase OH radicals from a liquid hydrocarbon and a liquid perfluorinated polyether (PFPE) has been investigated. The surfaces examined were the potentially reactive, branched hydrocarbon squalane ($C_{30}H_{62}$, 2,6,10,15,19,23-hexamethyltetracosane) and the inert PFPE Krytox 1506 ($F-[CF(CF_3)-CF_2O]_{14ave}-CF_2CF_3$). Superthermal OH was formed by 355-nm laser photolysis of a low pressure of HONO above the liquid surface. Laser-induced fluorescence (LIF) was used to determine the relative yields and nascent translational and rotational distributions of OH ($v' = 0$). The time-of-flight profiles from both liquids can be resolved, at least empirically, into two components. The dominant, faster component is consistent with direct, inelastic scattering. It has a higher average translational energy from PFPE than from squalane. This faster OH also has a higher Boltzmann-like rotational temperature for PFPE (655 ± 45 K) than for squalane (473 ± 27 K), in both cases considerably hotter than the incoming OH. For both liquids, there is also a slower component, with characteristics consistent with a thermalized, trapping-desorption mechanism. This is a higher proportion for squalane (0.22 ± 0.02) than for PFPE (0.09 ± 0.01). These results are consistent with squalane being the "softer" surface, exhibiting more efficient momentum transfer than PFPE, and more able to temporarily trap OH. Relative to PFPE, around half (0.49 ± 0.04) of the OH molecules that collide with squalane are lost, presumably due to reaction forming H_2O. These results are compared with previous studies of the scattering of inert gas species from both squalane and PFPE. The reactive branching fraction of OH on squalane is discussed in the context of previous observations of enhanced reactivity at the gas−liquid interface.

Introduction

Interactions at the gas−liquid interface are of fundamental importance in a great variety of processes, spanning diverse fields including respiration, atmospheric chemistry, distillation, and combustion. In atmospheric chemistry, a particular example concerns hydroxyl radicals, which act as key oxidants serving to "cleanse" the air. This beneficial action is both through homogeneous reactions with volatile organic compounds (VOCs),[1] and heterogeneously with organic components adsorbed on the surfaces of aerosol particles. The oxidation of the organic fractions of aerosols is also a key step in the development of their activity as cloud condensation nuclei.[2] The molecular-level dynamics of such processes therefore play a central role in the fundamental understanding of heterogeneous atmospheric chemistry.

Considerable progress has been made in the last 30−40 years in understanding the dynamics of the corresponding gas−*solid* interactions. Much of this has been afforded by improvements in experimental techniques. However, it is yet to be matched by equivalent progress in understanding interactions at the gas−liquid interface. This is mainly due to practical issues surrounding the maintenance of liquids under vacuum and the characterization of their surfaces. Despite these challenges, a number of studies have now been carried out. In particular, inelastic scattering of gases from liquid surfaces[3–22] and at the closely related surfaces of self-assembled monolayers[23–28] (SAMs) has been the focus of the majority of recent work. Reactions at the gas−liquid interface have received less attention, but this situation is also beginning to change.[29–42]

Inelastic scattering of gases from liquid surfaces has largely been investigated using atomic and molecular beams of closed shell species. Early work in the field was dominated by Nathanson and co-workers,[3–7] who scattered noble gas atoms from a number of liquids. These included both the branched, long-chain hydrocarbon squalane and a perfluorinated polyether (PFPE) of particular relevance in the current work. The recoiling atoms were detected using a rotatable quadropole mass filter, yielding their final, angle-dependent translational energies. The dependence of the scattering dynamics on a number of parameters was investigated, including the identity of the rare gas, energy and angle of impact, and liquid temperature, providing information on the scattering mechanism.

A common theme linking all such studies is the empirical identification of a bimodal translational energy distribution in the scattered species. The first, faster component has been assigned to direct, impulsive scattering (IS), where the interaction time is short and limited to one or, at most, a few collisions. Molecules leave the surface with a relatively high kinetic energy related to their initial energy. The second, slower feature is consistent with trapping-desorption (TD), where molecules are trapped at the surface for a sufficient time for them to be thermally accommodated, before escaping with a Maxwell−Boltzmann distribution of velocities. The two components can be considered as limiting cases of a continuum from a single through to a very large number of encounters of the gas molecule with the surface. This is reflected in realistic molecular dynamics simulations, particularly on more ordered model SAM surfaces.[43–47] These simulations are very successful in reproducing the observed inelastic scattering data from a range of SAMs. They have demonstrated, in particular, that the unique association of slower products with a TD mechanism may well be an

* Corresponding author. E-mail: k.g.mckendrick@hw.ac.uk.

10.1021/jp8024683 CCC: $40.75
Published on Web 06/26/2008

oversimplification. While it therefore remains a useful phenomenological way of categorizing experimental data, any apparent binary IS/TD separation should be interpreted with caution.

Beyond the noble gases, there have also been studies of the scattering of a number of neutral and ionic molecular species from liquids. These include CF_3^+, CF_2^+, and CF^+ from PFPE surfaces,[8–10] I_2 from both PFPE and squalane,[11,12] CO_2 from PFPE, glycerol, and squalane,[13–15] and HCl, CH_4, NH_3, and D_2O from glycerol and sulfuric acid.[16–22] Molecular projectiles obviously add a further dimension of partitioning the collision energy into *internal,* rotational, and vibrational modes of the scattered species. In high-energy (50−500 eV) collisions of CF_3^+, CF_2^+, and CF^+, this is sufficient to cause their dissociation on colliding with a liquid fluorocarbon surface.[8–10] The degree of dissociation increases with higher collision energies, larger CF_x groups, and wider total scattering angles. By analyzing the scattered velocities, it is possible to determine an effective mass for the liquid surface, indicating the effective dimensions of the section of the PFPE molecule that interacts with the incoming species. On this basis it was concluded that individual CF_x groups of the PFPE molecule protrude into the vacuum. This is corroborated by the noble gas scattering discussed above,[5,7] by independent angle-resolved photoelectron spectroscopy[48,49] and by more recent secondary-ion mass spectrometry.[50] The CF_x groups are thus believed to reside preferentially in the topmost layer of the PFPE surface, shielding the oxygen atoms below.

Of particular relevance to the current work are the investigations by McCaffery and co-workers[11,12] of inelastic scattering of molecular beams of I_2 from several liquids, including PFPE and squalane. The quantum-state distributions of I_2 were determined before and after collision with the surface using time-resolved laser-induced fluorescence (LIF). IS and TD channels were again clearly identified.

More recently, Nesbitt et al.[13–15] have developed a distinct spectroscopic technique for the detection of quantum state-resolved products of gas−liquid scattering. Collisions of supersonically cooled molecular beams of CO_2 with liquid PFPE, squalane and glycerol were studied by infrared absorption spectroscopy with sub-Doppler resolution. The translational, vibrational and rotational state distributions of the incident and scattered fluxes were measured. Internal rotational states and translational distributions were, once again, bimodal.

The works above set the context for the current study, where we seek to gain further insight into differences between scattering from the hydrocarbon squalane and from PFPE. The principal novelty lies in this being the first investigation of inelastic scattering of a potentially *reactive* molecular species, in this case the open-shell radical OH. We continue to build on previous studies of reactive and inelastic gas−liquid scattering of $O(^3P)$. These include the ground-breaking molecular-beam experiments of Minton,[29–33] and our own novel use of LIF to detect nascent OH radicals produced in $O(^3P)$ reactions at squalane and other liquid hydrocarbon surfaces.[34–36,38–40] Detection via LIF yields unique information on the internal energy distributions, along with broadly resolved translation energies. This complements the non-state-specific but much more highly resolved velocity measurements of Minton's group using molecular beams, which thus yielded, for example,[32] an effective mass for the squalane surface according to the same principles described above for PFPE.

In contrast to our previous work, in this study the *incoming* gas species is OH. We aim to determine the rotational distributions of OH scattered from both squalane and PFPE surfaces, along with measurements of the time-of-flight (TOF) appearance profiles, at a controlled liquid temperature. The relative intensities of the signals from the two liquids should reveal whether any OH is lost at the squalane surface. We interpret these results, drawing on previous studies of inelastic scattering of inert molecules and complementary results from $O(^3P)$ reactions with squalane and other hydrocarbons. We hope to reveal important new insight into the gas−liquid interfacial dynamics of OH of relevance, for example, to its key role in the atmosphere.

Experiment

A detailed description of the experimental apparatus has been published previously,[35] so only a brief outline is presented here. The primary vacuum chamber houses the heart of the experiment, a 5 cm-diameter stainless steel wheel. The wheel was partially immersed in a copper bath filled with the liquid under investigation. The wheel rotated at 0.5 Hz, creating a continuously refreshed liquid surface. The liquids used were the commercially available PFPE, Krytox 1506 ($F-[CF(CF_3)-CF_2O]_{14ave}-CF_2CF_3$), and squalane ($C_{30}H_{62}$, 2,6,10,15,19,23-hexamethyltetracosane). For an initial set of experiments verifying the source of the scattered OH, perdeuterated squalane ($C_{30}D_{62}$) was also used. The temperature of the bath was controlled at 298 K by a Peltier element, as in previous studies.[35]

OH radicals were generated from a gaseous nitrous acid (HONO) precursor, which was prepared in separate experiments by one of two methods. The main "salt−acid" method involved a reaction between sulfuric acid and sodium nitrite solution. H_2SO_4 (50 mL, 2M) was placed in a three-necked flask within an ice bath. $NaNO_2$ (100 mL, 2 M), held in a dropping funnel above, was added slowly to the acid at a constant drop rate of typically 0.25 drops/s. This yields HONO according to the reaction:

$$2NaNO_2(aq) + H_2SO_4(aq) \rightarrow 2HONO(g) + Na_2SO_4(aq)$$

The reaction was left to stabilize for at least 1 h before admitting gas to the vacuum chamber. The HONO gas evolved was extracted from the flask using a constant flow (∼50 sccm) of high-purity nitrogen. As a safety precaution, to avoid a build up of pressure in the flask, most of this flow was directed to exhaust, aside from a small fraction that was admitted to the vacuum chamber via a needle valve to achieve a precisely controlled constant pressure (nominally 1 mTorr). The N_2 flow rate was set to maximize HONO concentration (verified by LIF signal intensity of the photolytically produced OH) in the chamber while ensuring a sufficiently high throughput to prevent HONO decomposing to NO_2. Avoiding NO_2 formation was crucial, as this would also be photolyzed at 355 nm to yield $O(^3P)$. This would in turn react with squalane to produce OH, which would therefore be difficult to distinguish from the desired inelastically scattered OH. In practice we confirmed that negligible amounts of NO_2 were formed from this method of precursor generation in a series of tests with deuterated squalane (see below).

While this represented the main method we used to prepare the HONO precursor, an alternative, [51–53] based on the equilibrium

$$NO_2(g) + NO(g) + H_2O(l) \leftrightarrow 2HONO(g)$$

was also used for some experiments, because it is more convenient in practice than the salt−acid reaction. We proceeded by adding deionized water (10 mL) to a 12 L glass bulb. Following evacuation of the bulb, 1 atm of NO_2 (containing NO as an impurity) was added and left overnight to equilibrate.

The resulting gaseous mixture, which contained H_2O, NO_2, NO, and HONO in unknown proportions, was admitted to the chamber at the desired total pressure (~1 mTorr) using a needle valve. An advantage of this method was that it provided a very stable pressure over a long period; however, a major drawback is that a significant fraction of NO_2 is always present in the mixture. We therefore only used it for a set of experiments in which OH was scattered from PFPE, where $O(^3P)$ could not react to enhance the OH yield. When it was necessary to draw direct comparisons between OH scattering from PFPE and squalane, the principal NO_2-free, salt−acid method of HONO production was always used.

Regardless of the method of preparation, HONO was photolyzed in the vacuum chamber using the third harmonic of a Nd:YAG laser (Continuum Surelite SLII−10) at 355 nm, with a typical energy of 110 mJ in a nominal ~5 ns pulse. HONO photolysis at this wavelength has an anisotropy parameter, $\beta = -0.9$.[53] A $\lambda/2$ waveplate was therefore inserted into the photolysis beam path to rotate its linear polarization to vertical in the laboratory frame. This optimized, as far as is possible for a β close to the limiting value of −1, the recoil of OH toward the liquid surface. The distance of the wheel from the center of the (common) laser axis was set at a precisely controlled distance of 9 mm.

OH radicals were probed by LIF, including the primary products of the photolysis and, at later times, a proportion of those that have rebounded from the surface. LIF was excited on the $A^2\Sigma-X^2\Pi$ (1,0) band using a Nd:YAG (Continuum Surelite II-10) pumped dye laser (Sirah Cobra Stretch). This supplied 4−6 ns, ca. 0.5 mJ pulses, measured at the entrance to the vacuum chamber. The fluorescence emitted by the electronically excited OH radicals was collected by a liquid light guide (Ultrafine Technology, Ltd.) mounted 15 mm directly above the common laser axis. The fluorescence passed through custom interference filters before being converted into a signal by a photomultiplier tube (PMT; Electron Tubes, Ltd.). This signal was in turn digitized and passed to a PC, which collected data and controlled the wavelength and timing of the lasers using custom-written LabVIEW programs.

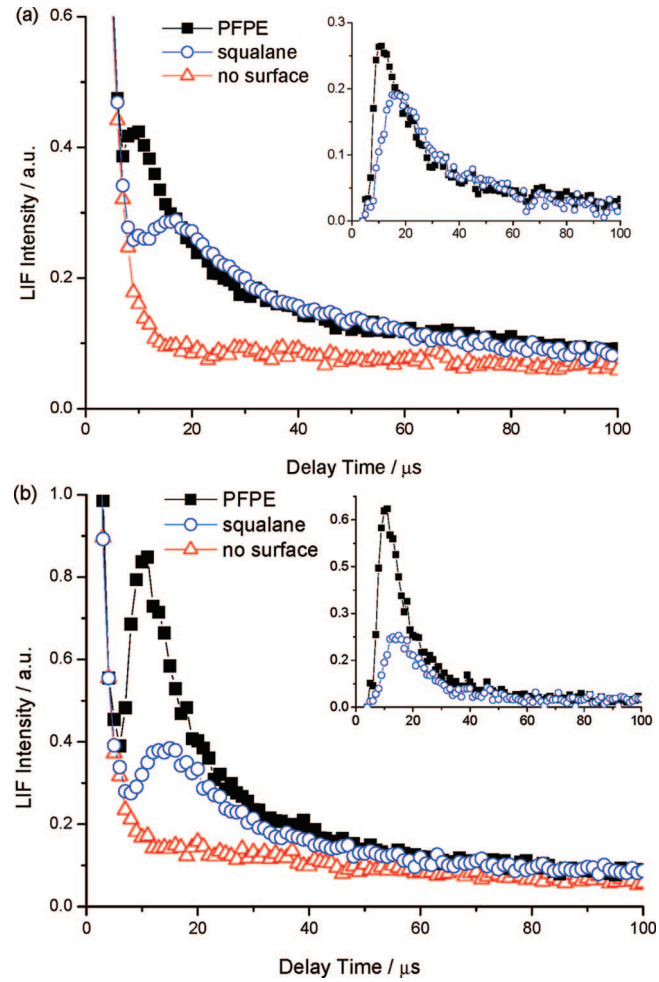

Figure 1. Measured appearance profiles of OH ($v' = 0$) raw LIF signals for PFPE liquid (filled squares), squalane (open circles), and with no liquid surface (open triangles). Profiles were recorded on the (a) $Q_1(1)$; and (b) $Q_1(5)$ lines of the OH A−X (1,0) band. Signals on each line are normalized at 4 μs. Bath temperature = 298 K; p(HONO mixture) ~ 1 mTorr; surface-probe laser distance = 9 mm. Insets show results of subtraction of the background (no liquid surface) from each of the PFPE and squalane data.

Results

OH Signal Verification. The first key goal was to identify unambiguously OH molecules that had collided with the liquid surfaces. Figure 1 shows OH ($v' = 0$, $N' = 1$ and 5, F_1) appearance profiles for both liquids. Also included is the photolytically generated OH background signal, which was recorded by removing the liquid-covered wheel (but not the assembly in which it is mounted or any other components) from the apparatus. It shows the decay of the photolytically generated OH, as well as any other contributions. These would include OH that has scattered from other adjacent parts of the apparatus, or with other gas-phase molecules, and returned to the probe volume. There are also minor, time-independent contributions from OH that is generated by photolysis of HONO by the probe laser itself. Scattered-light from the probe laser contributes an additional small constant offset, while any scatter from the photolysis laser contributes only at earlier times than are plotted in Figure 1.

The signals from both liquids (an average of ~8 individual profiles) and the background profiles have been scaled to a common value at 4 μs. At this early time, no OH can have collided with and returned from the liquid surface. Therefore normalization at this point accounts for any fluctuations in OH production due to precursor pressure, photolysis laser power, and so forth. The profiles recorded in the presence of either liquid clearly exhibit a distinct secondary maximum preceding a slowly decaying tail. We attribute these peaks to OH species scattering from the liquid surfaces. The arrival times of >9 μs are consistent with the approximate round-trip time expected on the basis of the velocities for OH species traveling to and from the liquid surface to the laser axis. They are seen very clearly in the insets of Figure 1, which show each of the profiles after subtraction of the background, revealing *only OH that has scattered from the liquid*.

We note that we have not attempted to monitor OH $v' = 1$ in the current work. It is known[53] that HONO photolysis at 355 nm produces very little vibrationally excited OH, and we did not expect significant upward scattering from $v' = 0$ to $v' = 1$ at our collision energies.

HONO Purity. As stated above, two methods were used to produce the gaseous HONO precursor. As we have explained, for experiments with squalane, it was essential to ensure that negligible NO_2 was present in the HONO mixture produced from the salt−acid reaction. To quantify the level of NO_2 present in this precursor mixture, an initial set of experiments was carried out using liquid $C_{30}D_{62}$. The total yield of OD detected from photolysis of the HONO mixture above $C_{30}D_{62}$ was

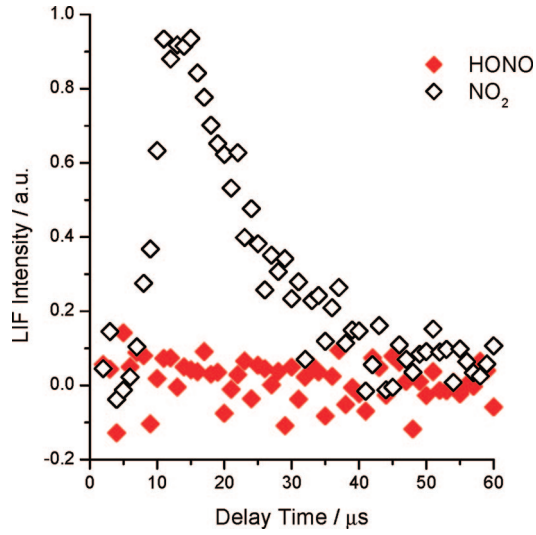

Figure 2. Measured appearance profiles of OD ($v' = 0$) LIF signal from photolysis of HONO mixture from salt−acid method (filled symbols) and pure NO_2 (open symbols) above a liquid perdeuterated squalane surface. Background probe and photolysis laser signals have been subtracted. Profiles were recorded on the $Q_1(1)$ line of the OD A−X (1,0) band. Bath temperature = 298 K; p(HONO or NO_2) ~ 1 mTorr; surface-probe laser distance = 5 mm.

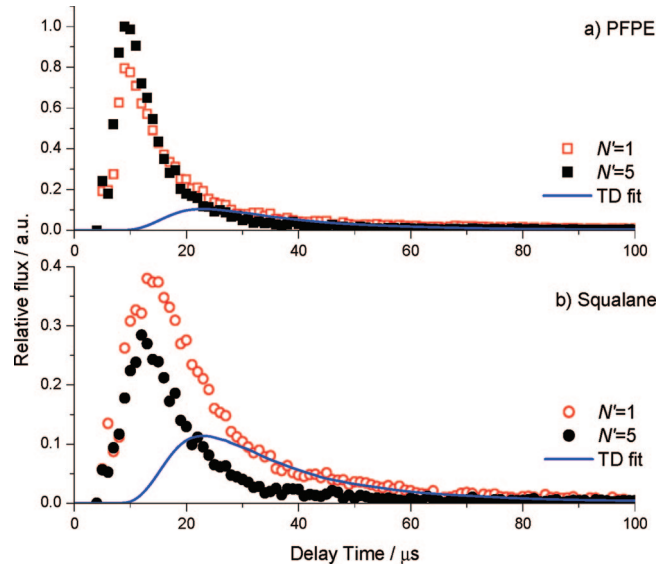

Figure 3. Measured appearance profiles of OH ($v' = 0$) scattered from (a) PFPE and (b) squalane. Recorded on the $Q_1(1)$ and $Q_1(5)$ lines of the OH A-X (1,0) band, scaled to indicate the correct relative populations in each level as discussed in text. Blue lines are simulated TD components fitted to the $N' = 1$ data (see Discussion). Signals (and the simulation) have been inversely time-weighted to reflect fluxes (see text), and with respective background signals subtracted. Bath temperature = 298 K; p(HONO) ~1 mTorr; surface−probe distance = 9 mm.

compared with that from a reference of essentially pure (98%) NO_2 above the same surface (as in our previous $O(^3P)$ + hydrocarbon experiments[34–36,38–40]). Figure 2 shows appearance profiles for OD using each of these precursor gases. While a significant OD signal was seen with 1 mTorr NO_2, on switching to the same pressure of the HONO mixture from the salt−acid method, essentially no OD was detectable within the signal-to-noise ratio. This result was confirmed over nine experiments on three different days, allowing us to set an upper limit of ~2−4% on the amount of NO_2 present in HONO produced by the salt−acid method. We can therefore be confident that the reaction of $O(^3P)$ made a negligible contribution to the scattered OH we observed from normal squalane.

As further confirmation of the source of the peaks in the appearance profiles (Figure 1), we verified that increasing the surface−probe distance resulted in a shift to later times, consistent with a longer round-trip distance of the scattering OH species. There was also a concurrent drop in signal intensity noted, as expected for straightforward geometric reasons. A similar signal verification procedure was carried out in earlier work.[35]

Comparison of Appearance Profiles: Squalane vs PFPE. Figure 3a,b presents in a revised form the measured appearance profiles for OH scattered from each of squalane and PFPE, probed on the $Q_1(1)$ and $Q_1(5)$ lines. As for the insets in Figure 2, the background signals have been subtracted to leave solely OH that has scattered from the liquid surface. The difference is that here the signals have been converted (approximately) to fluxes, to allow quantitative comparison of the total yield of scattered OH from the two liquids. This has been done simply by dividing the relative LIF intensity at each point, which is proportional to number density, by its appearance time. This accounts for the fact that the fastest OH molecules spend the least time in the probe beam region. We have neglected the distribution of arrival times at the surface resulting from the spatial extent of the photolysis beam. This has a negligible effect except at the very earliest times and does not materially affect the comparison of total fluxes from the liquids.

It is clear from Figure 3 that, while more OH scatters from PFPE (note the y-axis scaling, reflecting the raw signal ratios in Figure 1), a significant fraction still escapes the potentially reactive squalane surface. It is also instructive to compare OH yields measured on different rotational lines for the same liquid. To place these on the correct relative scale, we have accounted not only for the line-dependent background photolysis signals, as described above, but also for possible differences in detection sensitivity on the two lines. To achieve this, we recorded a LIF excitation spectrum at a time delay of 4 μs, probing purely the photolytically generated OH prior to any collisions with the surface. This was calibrated against a thermalized OH spectrum obtained in a separate experiment with a relatively long delay (30 μs) with a significant pressure (50 mTorr) of N_2 buffer gas added, as described previously.[34] The relative intensities of the $Q_1(1)$ and $Q_1(5)$ lines in the two spectra was combined with the known thermal ratio of populations (1:0.22) in the $X^2\Pi$ state levels probed by these transitions to establish the correct population ratio in the photolytic distribution (1:0.28). This was then used to scale the ratio of $Q_1(1)$ to $Q_1(5)$ appearance profiles at 4 μs, so that they correctly reflected relative populations. This correction has been applied in Figure 3, prior to the density-flux transformation.

Considering the two rotational levels in detail, it is clear that more OH scatters into $N' = 5$ than $N' = 1$ for PFPE, while for squalane the reverse is true. This immediately indicates that the OH scattered from PFPE is rotationally hotter than from squalane, a point we return to below. A further distinction between the signals is that the peak arrival time from PFPE is earlier than from squalane, corresponding to a higher average OH translational energy. For PFPE, it is clear that the two final rotational states have relatively similar translational distributions, with distinctive sharp profiles peaking at a common delay of around 9−10 μs. For squalane there is a larger distinction between the profiles, with $N' = 1$ more obviously gaining over $N' = 5$ at later times. These observations are explored in further

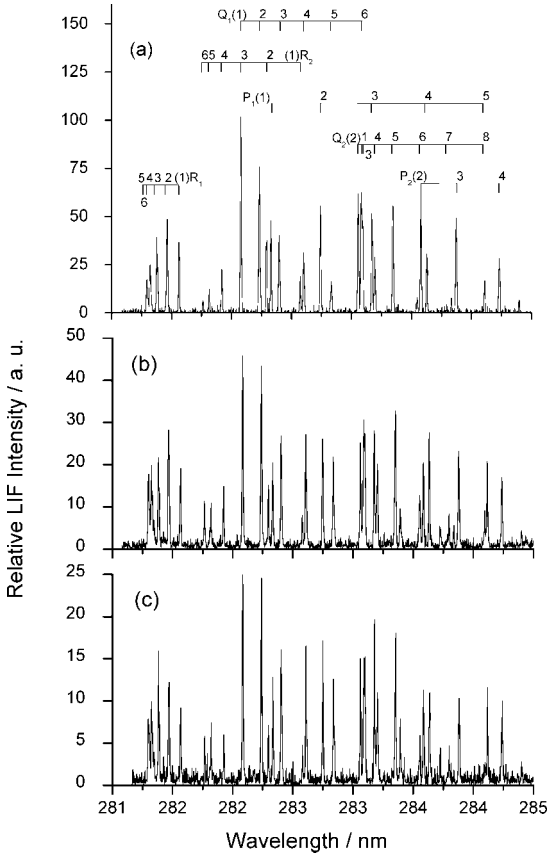

Figure 4. Representative OH A−X (1,0) LIF excitation spectra recorded at (a) photolytic creation (4 μs delay), (b) post-collision with PFPE (11 μs delay) and (c) post-collision with squalane (16 μs delay). Time delays in (b) and (c) correspond to peaks in the appearance profiles (Figure 1) for scattering from each liquid. Bath temperature ~298 K, p(HONO) ~1 mTorr; surface−probe distance = 9 mm.

detail below, where we also explain the simulated curves included in Figure 3.

Rotational Temperatures. The appearance profiles presented above are necessarily specific to particular rotational lines, in this case $Q_1(1)$ and $Q_1(5)$, so only give limited information on the rotational branching. To get a fuller picture of rotational energy transfer in the scattering process, we have measured rotational distributions at fixed delays: for the initial, photolytically produced OH (4 μs) and at the peak of scattered signal for both liquids. Figure 4 shows example LIF excitation spectra for these three cases, illustrating the relatively high signal-to-noise ratio achievable. Careful visual inspection shows that the photolytic distribution is perceptibly colder than that from scattering off either liquid.

In previous publications, we have deduced straightforward Boltzmann temperatures from such rotational distributions to allow direct comparison with the liquid surface temperature.[34–36,39,40] However, in the current work the rotational distributions obtained at the peaks of the appearance profiles are not composed solely of OH that has scattered from the liquid; there is an appreciable underlying contribution from the tail of the photolytically produced OH (see Figure 1).

We made use of the appearance profiles to carry out the necessary correction to the rotational distributions. We proceeded by first analyzing each of the spectra, making use of a thermalized calibration spectrum as described above and previously,[35] to extract the rotational populations in the lower levels probed by the Q_1 branch. This branch was chosen because of the strong intensities and good separation of the lines. We found similar distributions from all the main P, Q, and R branches, probing both Λ-doublets and spin−orbit manifolds, in the scattered spectra. The populations from the photolytic background spectrum were somewhat dependent on the branch probed, consistent with the known non-statistical populations produced in HONO photolysis.[53] These differences did not materially affect any conclusions reached from the comparison of squalane with PFPE, and the photolytic distribution is always considerable colder than either of them, regardless of the branch probed.

The resulting populations extracted from Q_1 branches at the peak of each appearance profile and at 4 μs are shown in Figure 5. In each case, the red columns indicate the populations at the peak, representing a combination of scattered and underlying photolytic signals. The green columns are the corresponding photolytic populations measured at 4 μs (which are in reasonable agreement with those reported previously[53]). The ratio between the pure photolysis signal and the combined signal at the peak of the profile was then determined from Figure 1. As a check on the procedure, we established these ratios independently for the both the $Q_1(1)$ and $Q_1(5)$ lines, because in principle both should yield the same final scattered populations. The ratio was used to subtract in each case the correctly weighted contribution of photolytic populations from the measured total populations at the peaks. This leaves solely the populations of OH that has scattered from the surface, shown as blue columns in Figure 5 for the subtractions based on each of the normalizations to $N' = 1$ and 5, respectively.

As can be seen from Figure 5, the final scattered distributions derived from the $N' = 1$ and $N' = 5$ calibrations for each liquid are in reasonably good agreement. There are much more significant differences between the distributions for squalane and PFPE. These observations are reflected in the corresponding best-fit rotational temperatures to the various distributions, listed in Table 1. The results confirm the qualitative observation above that OH molecules scattered from both PFPE and squalane are rotationally hotter than the photolytic pre-collision species. These differences are naturally amplified when the underlying photolytic contribution has been removed. Furthermore, those scattered from PFPE are seen to be significantly rotationally hotter than from squalane, again exposed more clearly by subtraction of the background.

Armed with the rotational temperatures in Table 1, the appearance profiles in Figure 3 can be used to estimate the overall fraction of OH lost, presumably by reaction to form H_2O, at the squalane liquid surface. It is assumed that scattering from PFPE represents 100% survival of OH. The relevant temperature is used to correct for the fraction of the total population that ends up in the rotational level probed in each profile. On this basis, the $N' = 1$ profiles imply that the overall fractional loss, summed over all rotational levels, at the squalane surface is 0.42 ± 0.08. The corresponding fraction based on $N' = 5$ is 0.51 ± 0.05. This gives a weighted mean best estimate for the loss of OH on squalane close to one-half (0.49 ± 0.04), where all uncertainties quoted are 1σ errors based purely on statistical variations (including the effects of the uncertainties in the rotational temperatures).

Discussion

We have for the first time monitored superthermal OH radicals pre- and post- collision with liquid squalane and PFPE surfaces. LIF detection has provided comparative yields, along with translational and rovibrational internal energy distributions.

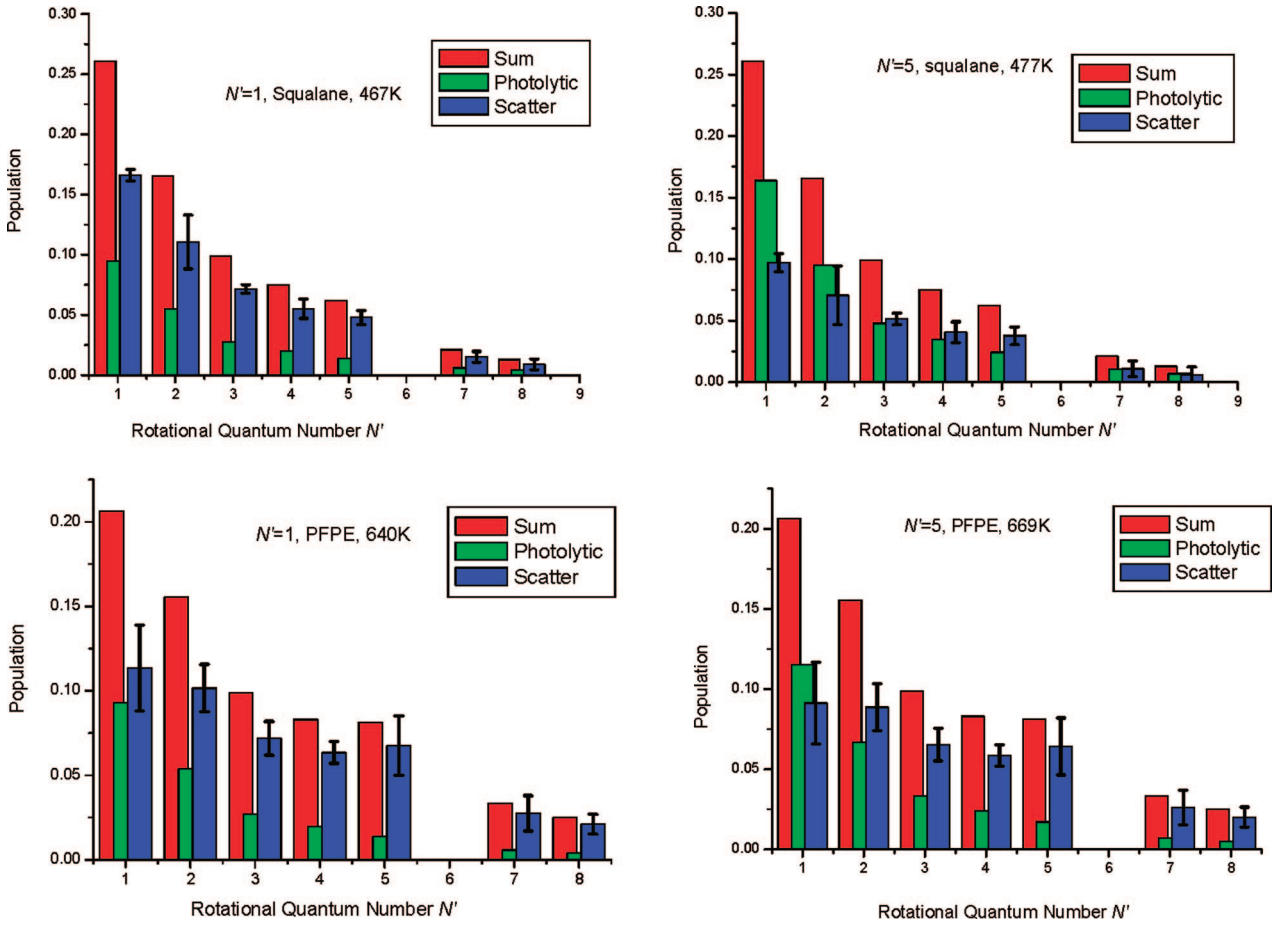

Figure 5. Rotational populations deduced from the Q_1 branch for OH as formed photolytically at 4 μs (green), at the peaks of the appearance profile (11 μs for PFPE and 16 μs for squalane) (red), and the differences between the two following scaling based on normalization (see text) to either $N' = 1$ or 5 (blue). Error bars represent combinations of the errors (1σ) in the average populations from three independent excitation spectra at each delay. ($N' = 6$ is absent because the $Q_1(6)$ line is blended.)

TABLE 1: Rotational Temperatures of OH ($v'=0$) as Formed Photolytically, Combined Signals at Peak, and Subtracted Scattered Signals from PFPE and from Squalane[a]

T_{rot}/ K	background scaled at	PFPE	squalane
photolytic		329 ± 35	329 ± 35
combined signal at peak		484 ± 56	420 ± 43
scattered signal (photolytic	$N' = 1$	640 ± 65	467 ± 44
background subtracted)	$N' = 5$	669 ± 61	477 ± 35
	weighted average	655 ± 45	473 ± 27

[a] Determined from the F_1 manifold of levels probed by the Q_1 branch, measured at 4 μs (photolytic), 11 μs (PFPE) and 16 μs (squalane). Each temperature and associated error is the result of averaging three individual measurements for both the photolytic and scattered distributions. Bath temperature = 298 K.

The branching between OH radicals that *escape* from the squalane surface and those that are implicitly *lost* there is deduced by comparing the yield from squalane with that from PFPE, for which we assume there are no significant loss mechanisms. Of those that escape either surface, there may, in principle, be contributions from distinct mechanisms. As discussed in the Introduction, the two widely invoked limiting cases are IS and TD. We attempt below at least a phenomenological separation into contributions of this type on the basis of their different translational and internal energy distributions.

Translational Distributions. Leaving aside for the moment the OH species lost in the surface, we first consider those radicals that escape and are detected. As we have noted, an obvious difference between the liquids is that OH scatters with a higher average translational energy from PFPE than from squalane (see Figures 1 and 3). The mean laboratory-frame translational energy of OH radicals formed from the HONO photolysis[53] is 53.7 kJmol^{-1}, equivalent to a speed of 2,520 ms^{-1}. At this speed, the impinging OH radicals will travel the 9 mm to the liquid surface in an average time of 3.6 μs. The time taken for the scattered OH radicals to travel the same distance back to the laser axes can be estimated crudely by subtracting 3.6 μs from the peak arrival time in the appearance profile ($\sim$9 μs for PFPE and $\sim$15 μs from squalane). This yields a most-probable scattered velocity of 1660 ms^{-1} for OH scattered from PFPE and 790 ms^{-1} from squalane. There is admittedly considerable geometric blurring in the current experiment (see below), and in particular any average angle that the incoming and outgoing velocities might make with the surface normal is being neglected in making these simple estimates, which would lead to the recoil speeds being underestimated. Nevertheless, they clearly indicate that OH molecules scattered from squalane are moving considerably more slowly than those scattered from PFPE.

As we also justify further below, at these relatively short peak arrival times, the scattering must be dominated by the IS channel. The energy transferred to the liquid surface in these inelastic collisions can be estimated roughly from the difference between the average energies (including a minor contribution from rotation based on the rotational temperatures in Table 1) of the incoming and recoiling OH. Expressing the energy lost

to the surface (ΔE_{IS}) as a fraction of the initial incoming (translational plus rotational) energy E_i, energy transfer fractions ($\Delta E_{IS}/E_i$) in the IS channel are found to be ~0.49 for PFPE and ~0.84 for squalane. These are likely to be overestimates for the reasons just discussed. They can be compared with the previous results of Nathanson et al.[5–7] who explored impulsive energy transfer to PFPE and squalane liquid surfaces in molecular beam experiments for species of similar mass to OH (Ne, CH_4, NH_3 and D_2O). The transfer fractions, based on translational energy only, were reassuringly similar to those found here when the collision energies nearest to our own (54 kJ mol^{-1}) are compared: e.g., 0.43 for Ne to PFPE at 60 kJ mol^{-1}, and 0.57 and 0.64 for Ne at 60 kJ mol^{-1} and D_2O at 66 kJ mol^{-1}, respectively, to squalane. The overall trends in the TOF spectra in the molecular beam experiments were also similar to the appearance profiles we report here; scattering from PFPE gives a sharp peak with rapidly decaying tail, while, from squalane, the peak is both later and broader. We conclude that PFPE presents a stiffer, more elastic surface than squalane to the incoming OH radicals, as had previously been found for inert atoms and molecules. A similar distinction between hydrocarbon and fluorocarbon liquid surfaces has also been seen in the spectroscopically based studies with I_2[11,12] and CO_2[13–15] as the impinging species.

The broader shape of the appearance profiles for squalane suggests the possibility of a significant TD component. We have simulated the expected form of a TD component by a Monte Carlo method, similar to the type we have described previously.[35] In essence, OH trajectories that originate in the photolysis volume and intercept the liquid surface were Monte Carlo sampled from the known photolytic OH velocity distribution.[53] This defined a flight time to the surface, and starting coordinates for the return leg. In the absence of a known angular scattering distribution, it is not possible to simulate IS scattering. For the TD component that we are considering here, trajectories for the desorbing OH were Monte Carlo sampled from a Maxwell−Boltzmann velocity distribution, with the usual assumption of a cos θ-weighted angular distribution about the surface normal. They were counted as successful if they intercepted the probe laser volume viewed by the liquid light guide. The total flight times from photolysis to both entry and exit from the probe volume, for each combined trajectory, were collected for a large number of successful iterations. The appearance profile was then simulated as being directly proportional to the instantaneous OH density in the probe volume at each time. This exactly matches what is measured in the experiment, including the significant distribution of pathlengths traveled from the surface to the probe region, which is the main source of geometric blurring of arrival times.

The simulations thus mimic the raw LIF appearance profiles of the type shown in Figure 1. We have in practice chosen to subject them to the same (approximate) density-flux transformation to allow them to be presented alongside the transformed experimental profiles in Figure 3. The simulated profiles have been fit to the long-time tails of the experimental appearance profiles, where TD would be expected to dominate. By integrating the resulting areas of the experimental and simulated profiles, it is possible to determine at least a nominal TD component for both liquids. In Figure 3 we only show for clarity the TD fits for the $N' = 1$ level. Similar fits were made for $N' = 5$. In principle, both fits should yield consistent overall TD fractions, in each case taking account of the different *rotational* temperatures of the IS (see Table 1) and TD (assumed 298 K) components and hence the fractions of each population in a given rotational level. The $N' = 1$ profiles produce an overall apparent TD component of 20 ± 3% for squalane and 10 ± 1% for PFPE. Repeating the procedure for $N' = 5$ profiles produces reassuringly similar TD components of 23 ± 2% for squalane and 8 ± 1% for PFPE. Bearing in mind the caution referred to in the Introduction[43–47] that should be exercised in inferring that all slow-moving molecules are necessarily associated at a microscopic level with trapped trajectories, our best overall empirical estimates of the fractions of our observed populations that have speeds consistent with a TD mechanism are therefore 22 ± 2% for squalane and 9 ± 1% for PFPE. Justifying our earlier statements above, close examination of the onset of the simulated TD components in Figure 3 suggests that at the peaks of the appearance profiles where the rotational temperatures were measured there can effectively be no underlying TD contribution for PFPE, and at most a very minor one for squalane.

We conclude that squalane is clearly not only better at dissipating the initial OH momentum, but also appears more effective at accommodating OH at the surface than PFPE. The factors controlling these two attributes have been discussed by Nathanson and co-workers[6] in the context of their previous molecular beam experiments with different colliders and liquids. They found an interplay between "softer" surfaces favoring efficient momentum transfer and strongly attractive interactions with the collision partner enhancing TD. At incident energies comparable to ours (and fixed incident and outgoing angles of 45°), the assigned TD fraction increased from ~10% to ~20% along the sequence Ne, CH_4, NH_3, and D_2O for PFPE. Consistent with our present results, it was systematically higher, ranging from ~20% to 40%, for the same species from squalane.[6] We would not necessarily have expected exact quantitative agreement with our apparent TD fractions. Quite apart from the distinct chemical identity of OH and the nature of its attractive interactions with the two surfaces, our measurements have a lower translational energy resolution. They may also be subject to a potential but unquantified selectively toward certain scattering angles (known to affect the IS:TD ratio[7]), although our MC simulations suggest this should be weak for the current relatively short probe-laser to liquid surface distances. Nevertheless, our results fit the general trend of previous observations that a comparatively smaller apparent TD component is found for PFPE than for squalane. Similar differences have been found for related SAM surfaces,[23–27] where we note again the caution provoked by the complementary molecular dynamics simulations[43–47] over too literal an interpretation of the empirical binary divide into only the two IS and TD limiting mechanistic types.

Rotational Distributions. The main advantage of our method over the molecular beam scattering experiments is the ability to access *internal* energy distributions. The corrected rotational temperatures in Table 1 demonstrate that OH scattered from either liquid at the peak of the appearance profile is substantially rotationally hotter (655 ± 45 K from PFPE, 473 ± 27 K from squalane) than the OH prior to its collision with the surface (329 ± 35 K, at least for the levels probed by the Q_1 branch as discussed above). This strongly supports the argument from the translational energy distributions that IS dominates the scattering at this point in the profile, with significant translational to rotational (T−R) energy transfer in impulsive collisions. The rotational temperature is clearly significantly higher from PFPE than from squalane. (As we have noted, this can be deduced simply from the relative magnitudes of the correctly weighted appearance profiles for $N' = 1$ and 5 for each liquid in Figure

3). This is also consistent with a stiffer PFPE surface leading to more efficient T−R transfer.

We can compare this aspect of our results to the very limited number of other studies of rotationally resolved scattering from liquids. Nesbitt et al. investigated scattering of CO_2 from squalane and PFPE.[13–15] A wide range of final *J*-states were detected, yielding Boltzmann plots that could be fitted to a two-temperature model. These were assumed to be a thermal TD component and a high-temperature IS one, in agreement with our observation here of rotational excitation in the IS component. Consistent with the qualification we have noted above,[44] a refinement to the basic picture of two discrete components was also proposed, whereby the IS channel may reflect both single and limited-multiple collisions as opposed to exclusively single, hard-sphere-type interactions. The apparent TD component was substantial, with the ratio shifting in favor of IS for increasing collision energy and more grazing CO_2-beam incidence angles and, necessarily, higher *J*-states. Perhaps of most relevance here, IS was favored for scattering of CO_2 from PFPE over squalane, which is consistent with our current results for OH. In the earlier works of McCaffery et al., I_2 was scattered from squalane and PFPE among other liquid/solid surfaces.[11,12] Both IS and TD features were identified. Squalane was found to be more effective at trapping I_2 at the surface, showing greater vibrational warming of the vibrationally (and rotationally) cold incident beam. For the IS component, although there was only relatively weak rotational warming from the initially cold distribution, the scattered I_2 was rotationally hotter from PFPE than from squalane. These observations are again in qualitative agreement with our results for OH in the current work.

The identification of a significant component consistent with a TD mechanism for OH scattering from squalane is an interesting observation. It might have been expected that accommodation and subsequent multiple collisions of a highly reactive species such as OH, starting from a high initial translational energy, would result in a high probability of hydrogen abstraction to form H_2O. Although, as we have quantified above and go on to discuss, a substantial fraction of the OH radicals do indeed appear to react with the squalane surface, our results demonstrate that some of the OH radicals that acquire thermal velocities do leave the surface intact. A recent kinetic study of the H-abstraction reaction for OH with a wide range of (gas-phase) alkanes determined typical activation energies in the range 3−10 kJ mol^{-1} depending on the primary, secondary, or tertiary nature of the C−H bond.[54] These are only slightly higher than thermal energies, suggesting that escape from the liquid must also be subject to relatively low effective barriers (related to the average trapping potential of OH at the squalane surface) and take place within a relatively small number of secondary encounters. The detection of OH with thermal energies in the current experiment is furthermore an important corroboration of our previous work on the reaction of $O(^3P)$ with squalane[34–36,39] and other hydrocarbons.[40] It supports the conclusions that we have drawn, most compellingly from the dependence of the OH rotational temperature on the liquid temperature but supported by the bimodal nature of the translational energy distributions, that OH formed by reaction of $O(^3P)$ with the hydrocarbon surface can survive sufficiently long at least to translationally and rotationally thermalize before desorbing.

Reaction of OH. We turn now to the fate of the OH which *does not* escape from the liquid surface. We have made the assumption that the observed integrated flux for PFPE is representative of an escape probability of 100% of the OH molecules that impact the surface. We are therefore neglecting, for example, any unknown differences in the angular scattering distributions of the IS components from PFPE and squalane to which our method might be sensitive. Within this assumption, we find that around half (49 ± 4%) of the OH molecules that collide with squalane do not survive. The most obvious fate of this lost OH is that it is has reacted to yield H_2O through simple hydrogen abstraction, as discussed above. H_2O has indeed been observed as a nascent secondary reaction product in the molecular beam experiments of Minton's group on $O(^3P)$ with squalane.[29–32]

The reaction probability of OH with organic surfaces is an important parameter for understanding, among other practically important phenomena, oxidation of atmospheric aerosols. A number of studies have attempted to investigate this key step, using a variety of techniques including droplet/bubble train flow reactors, aerosol chambers, and liquid jets.[55] A gap in the current understanding is the reason behind the widely observed enhanced reactivity at condensed phase surfaces over the equivalent gas-phase bimolecular processes[2,56–59] which has in some cases been reported to be many orders of magnitude.[55,60]

We note that there is a logical flaw in an oversimplified application of Arrhenius parameters for gas-phase bimolecular reactions to predict the rates of the corresponding gas−surface processes. The gas-phase *A*-factor will commonly be substantially smaller than the gas-kinetic collision frequency. A significant contribution to the difference comes from nonreactive collisions that are forward scattered. In the gas phase, such a collision is then over. However, for a collision at a surface, forward scattering will inevitably lead to a secondary encounter with the surface. This is an obvious source, at least for thermal energy collisions, of some degree of enhancement of the reactivity at the surface. If the secondary collision leads to trapping and multiple additional encounters, then the rate will be increased by a corresponding multiplicative factor.

Nevertheless, it remains unclear the extent to which this might at least partly explain the enhanced reactivity at surfaces. The magnitude of the effect is found to vary widely. For example, Moise and Rudich note that while the reactive uptake of Br on alkane surfaces is 10^4 times greater than in the equivalent gas-phase system, for Cl there is no enhancement at the liquid surface.[57] They suggest that only reactions with high gas-phase activation energies can be enhanced at surfaces, postulating that they are "catalyzed" on the surface, without specifying a mechanism by which that might operate.

Alternative explanations have proposed that the enhancement is due to the formation of surface complexes, surface photochemistry, or enhanced anion concentrations at the surface of aqueous salt solutions.[56] Many of these only relate to bulk kinetic systems, where the phenomenological loss of a reactant may be the result of a complex overall mechanism involving secondary reactions. In the case of OH, suggested mechanisms for the overall reaction with organic layers involve the copresence of O_2 and the initial creation of ketones, aldehydes, and carboxylic acids, which subsequently react with further OH.[61] Nevertheless, it is generally accepted that the initial step is a straightforward hydrogen abstraction, preceding secondary oxidation.[2] This initial elementary process is the aspect probed directly in our current study. Typical activation energies for H-abstraction are, as noted above,[54] in the range of 3−10 kJ mol^{-1} for a wide range of hydrocarbons. Their gas-phase Arrhenius *A*-factors are typically $\sim 10^{-11}$ cm^3 s^{-1} compared with a representative gas-kinetic collision rate constant of $\sim 3 \times 10^{-10}$ cm^3 s^{-1}, suggesting only 1 in 30 of the collisions with sufficient

energy result in reaction in the gas phase. For the reasons noted above, we would not expect this simplistic argument to be transferable to reaction at the liquid surface. Indeed our own results show at least an order of magnitude higher reactivity, with a reaction probability of 0.49 ± 0.04, for superthermal collisions which all, at least initially, have energies substantially above the activation barrier. This enhancement over the prediction based on the *A* factor is seen despite the relatively low barrier. Our measurement of the reactive fraction of collisions compares quite favorably with thermal-energy reactive uptake probabilities (γ) of OH on organic aerosol surfaces, which range from >0.1 to 1.[2,59,62,63] Similar values are found for solid $(NH_4)_2SO_4$ and NH_4HSO_4 surfaces exposed to trace pressures of 1-hexanol, increasing the reaction probability to >0.2 compared to $\gamma < 0.03$ for the untreated surfaces.[64] Consistent with our assumption that the PFPE surface is inert to OH, on halocarbon surfaces[2,63] the reaction probability is even lower, on the order of $10^{-3}-10^{-4}$. Through our current method we have provided an unambiguously elementary measurement of the reactive uptake of OH on a well-characterized liquid hydrocarbon surface, which may be of value in the mechanistic interpretation of more complex systems.

Conclusions

The bulk of the OH ($v' = 0$) scattered from a liquid PFPE surface has a significantly higher average translational energy than from liquid squalane. It is also rotationally hotter, with the OH scattered from both liquids having higher Boltzmann-like rotational temperatures than the incoming OH. These results are consistent with a predominantly direct, IS mechanism, with PFPE having the stiffer liquid surface.

Nevertheless, both liquids also show a minor, slower, and rotationally colder component, whose characteristics are consistent with a thermalized TD mechanism. The two liquids may be distinguished by a phenomenological resolution into IS and TD components, with only an estimated $9 \pm 1\%$ compatible with the TD mechanism from PFPE, compared to $22 \pm 2\%$ from squalane. The observation of this component for squalane is consistent with some OH surviving sufficiently long at the surface to be translationally and rotationally thermalized, despite the low barrier to hydrogen abstraction.

Relative to PFPE, around half ($49 \pm 4\%$) of the OH impacting on squalane is lost, presumably to reaction forming H_2O. A simplistic application of the gas-phase Arrhenius parameters for H-abstraction would suggest a far lower reaction yield. This may be relevant to previous observations of enhanced reaction probabilities of gas−liquid reactions over their gas-phase counterparts.

Acknowledgment. We thank the EPSRC for a research grant and studentship funding for C.W. M.L.C. is grateful to Research Councils U.K. for an Academic Fellowship.

References and Notes

(1) Kleinman, L. I.; Daum, P. H.; Imre, D.; Lee, Y. N.; Nunnermacker, L. J.; Springston, S. R. *Geophys. Res. Lett.* **2002**, *29*, 1467.
(2) Bertram, K.; Ivanov, A. V.; Hunter, M.; Molina, L. T.; Molina, M. J. *J.Phys. Chem. A* **2001**, *105*, 9415.
(3) King, M. E.; Fiehrer, K. M.; Nathanson, G. M.; Minton, T. K. *J. Phys. Chem. A* **1997**, *101*, 6556.
(4) Nathanson, G. M.; Davidovits, P.; Worsnop, D. R.; Kolb, C. E. *J. Phys. Chem.* **1996**, *100*, 13007.
(5) King, M. E.; Saecker, M. E.; Nathanson, G. M. *J. Chem. Phys.* **1994**, *101*, 2539.
(6) Saecker, M. E.; Nathanson, G. M. *J. Chem. Phys.* **1993**, *100*, 3999.
(7) King, M. E.; Nathanson, G. M.; Hanning-Lee, M. A.; Minton, T. K. *Phys. Rev. Lett.* **1993**, *70*, 1026.
(8) Koppers, W. R.; Beijersbergen, J. H. M.; Weeding, T. L.; Kistemaker, P. G.; Kleyn, A. W. *J. Chem. Phys.* **1997**, *107*, 10736.
(9) Koppers, W. R.; Gleeson, M. A.; Lourenço, J.; Weeding, T. L.; Los, J.; Kleyn, A. W. *J. Chem. Phys.* **1999**, *110*, 2588.
(10) Los, J.; Gleeson, M. A.; Koppers, W. R.; Weeding, T. L.; Kleyn, A. W. *J. Chem. Phys.* **1999**, *111*, 11080.
(11) Kenyon, A. J.; McCaffery, A. J.; Quintella, C. M.; Zidan, M. D. *J. Chem. Soc., Faraday Trans.* **1993**, *89*, 3877.
(12) Kenyon, A. J.; McCaffery, A. J.; Quintella, C. M.; Zidan, M. D. *Faraday Discuss.* **1993**, *96*, 245.
(13) Perkins, B. G., Jr.; Häber, T.; Nesbitt, D. J. *J. Phys. Chem. B* **2005**, *109*, 16396.
(14) Perkins, B. G., Jr.; Nesbitt, D. J. *J. Phys. Chem. B* **2006**, *110*, 17126.
(15) Perkins, B. G., Jr.; Nesbitt, D. J. *J. Phys. Chem. A* **2007**, *111*, 7420.
(16) Nathanson, G. M.; Davidovits, P.; Worsnop, D. R.; Kolb, C. E. *J. Phys. Chem.* **1996**, *100*, 13007.
(17) Morris, J. R.; Behr, P.; Antman, M. D.; Ringeisen, B. R.; Splan, J.; Nathanson, G. M. *J. Phys. Chem. A* **2000**, *104*, 6738.
(18) Ringeisen, B. R.; Muenter, A. H.; Nathanson, G. M. *J. Phys. Chem. B* **2002**, *106*, 4988.
(19) Ringeisen, B. R.; Muenter, A. H.; Nathanson, G. M. *J. Phys. Chem. B* **2002**, *106*, 4999.
(20) Chorny, I.; Benjamin, I.; Nathanson, G. M. *J. Phys. Chem. B* **2004**, *108*, 995.
(21) Muenter, A. H.; DeZwaan, J. L.; Nathanson, G. M. *J. Phys. Chem. B* **2006**, *110*, 4881.
(22) Muenter, A. H.; DeZwaan, J. L.; Nathanson, G. M. *J. Phys. Chem. C* **2007**, *111*, 15043.
(23) Gibson, K. D.; Isa, N.; Sibener, S. J. *J. Phys. Chem.* **2003**, *119*, 13083.
(24) Scott Day, B.; Morris, J. R. *J. Phys. Chem.* **2003**, *107*, 7120.
(25) Scott Day, B.; Morris, J. R. *J. Chem. Phys.* **2005**, *122*, 234714.
(26) Scott Day, B.; Morris, J. R.; Alexander, W. A.; Troya, D. *J. Phys. Chem. A* **2006**, *110*, 1319.
(27) Lohr, J. R.; Scott Day, B.; Morris, J. R. *J. Phys. Chem. A* **2006**, *110*, 1645.
(28) Tasić, U. S.; Yan, T.; Hase, W. L. *J. Phys. Chem.* **2006**, *110*, 11863.
(29) Garton, D. J.; Minton, T. K.; Alagia, M.; Balucani, N.; Casavecchia, P.; Volpi, G. G. *Faraday Discuss.* **1997**, *108*, 387.
(30) Garton, D. J.; Minton, T. K.; Alagia, M.; Balucani, N.; Casavecchia, P.; Volpi, G. G. *J. Chem. Phys.* **2000**, *112*, 5975.
(31) Garton, D. J.; Minton, T. K.; Alagia, M.; Balucani, N.; Casavecchia, P.; Volpi, G. G. *J. Chem. Phys.* **2001**, *114*, 5958.
(32) Zhang, J.; Garton, D. J.; Minton, T. K. *J. Chem. Phys.* **2002**, *117*, 6239.
(33) Zhang, J.; Upadhyaya, H. P.; Brunsvold, A. L.; Minton, T. K. *J. Phys. Chem. B* **2006**, *110*, 12500.
(34) Kelso, H.; Köhler, S. P. K.; Henderson, D. A.; McKendrick, K. G. *J. Chem. Phys.* **2003**, *119*, 9985.
(35) Köhler, S. P. K.; Allan, M.; Kelso, H.; Henderson, D. A.; McKendrick, K. G. *J. Chem. Phys.* **2005**, *122*, 24712.
(36) Köhler, S. P. K.; Allan, M.; Costen, M. L.; McKendrick, K. G. *J. Phys. Chem. B* **2006**, *110*, 2771.
(37) Köhler, S. P. K.; Reed, S. K.; Westacott, R. E.; McKendrick, K. G. *J. Phys. Chem. B* **2006**, *110*, 11717.
(38) Allan, M.; Bagot, P. A. J.; Köhler, S. P. K.; Reed, S. K.; Westacott, R. E.; Costen, M. L; McKendrick, K. G. *Phys. Scr.* **2007**, *76*, C42.
(39) Allan, M.; Bagot, P. A. J.; Costen, M. L.; McKendrick, K. G. *J. Phys. Chem. C* **2007**, *111*, 14833.
(40) Allan, M.; Bagot, P. A. J.; Westacott, R. E.; Costen, M. L.; McKendrick, K. G *J. Phys. Chem. C* **2008**, *112*, 1524.
(41) Zolot, A. M.; Harper, W. W.; Perkins, B. G.; Dagdigian, P. J.; Nesbitt, D. J. *J. Chem. Phys.* **2006**, *125*, 021101.
(42) Kim, D.; Schatz, G. C. *J. Phys. Chem. A* **2007**, *111*, 5019.
(43) Isa, N.; Gibson, K. D.; Yan, T.; Hase, W.; Sibener, S. J. *J. Chem. Phys.* **2004**, *120*, 2417.
(44) Martínez-Núñez, E.; Rahaman, A.; Hase, W. L. *J. Phys. Chem. C* **2007**, *111*, 354.
(45) Vázquez, S. A.; Morris, J. R.; Rahaman, A.; Mazyar, O. A.; Vayner, G.; Addepalli, S. V.; Hase, W. L.; Martínez-Núñez, E. *J. Phys. Chem. A* **2007**, *111*, 12785.
(46) Day, B. S.; Morris, J. R.; Troya, D. *J. Chem. Phys.* **2005**, *122*, 214712.
(47) Tasić, U.; Day, B. S.; Yan, T.; Morris, J. R.; Hase, W. L. *J. Phys. Chem. C* **2008**, *112*, 476.
(48) Ramasamy, S.; Pradeep, T. *J. Chem. Phys.* **1995**, *103*, 485.
(49) Pradeep, T. *Chem. Phys. Lett.* **1995**, *243*, 125.
(50) Lourenço, J. M. C.; Carrapa, R. T.; Teodoro, O. M. N.; Moutinho, A. M. C.; Gleeson, M. A.; Los, J.; Kleyn, A. W. *Chem. Phys. Lett.* **2001**, *336*, 431.
(51) Beck, R. D.; Rizzo, T. R. *J. Chem. Phys.* **2000**, *112*, 8885.

(52) Novicki, S. W.; Vasudev, R. *J. Chem. Phys.* **1991**, *95*, 7269.
(53) Vasudev, R.; Zare, R. N.; Dixon, R. N. *J. Chem. Phys.* **1984**, *80*, 4863.
(54) Wilson, E. W., Jr.; Hamilton, W. A.; Kennington. R.; Evans, B., III; Scott, N. W.; DeMore, W. B. *J. Phys.Chem. A* **2006**, *110*, 3593.
(55) Davidovits, P.; Kolb, C. E.; Williams, L. R.; Jayne, J. T.; Worsnop, D. R. *Chem. Rev.* **2006**, *106*, 1323.
(56) Moise, T.; Rudich, Y. *J. Geophys. Res., [Atmos.]* **2000**, *105*, 14667.
(57) Moise, T.; Rudich, Y. *Geophys. Res. Lett.* **2001**, *28*, 4083.
(58) Paz, Y.; Trakhtenberg, S.; Naaman, R. *J. Phys. Chem.* **1994**, *98*, 13517.
(59) Vione, D.; Maurino, V.; Minero, C.; Pelizzetti, E.; Harrison, M. A. J.; Olariu, R.-I.; Arsene, C. *Chem. Soc. Rev.* **2006**, *35*, 441.
(60) Molina, M. J.; Molina, L. T.; Kolb, C. E. *Annu. Rev. Phys. Chem.* **1996**, *47*, 327.
(61) Eliason, T. L.; Gilman, J. B.; Vaida, V. *Atmos. Environ.* **2004**, *38*, 1367.
(62) George, I. J.; Vlasenko, A.; Slowik, J. G.; Broekhuizen, K.; Abbatt, J. P. D. *Atmos. Chem. Phys.* **2007**, *7*, 4187.
(63) Rudich, Y. *Chem. Rev.* **2003**, *103*, 5097.
(64) Cooper, P. L.; Abbatt, J. P. D. *J. Phys. Chem.* **1996**, *100*, 2249.

JP8024683